ResearchGate

See discussions, stats, and author profiles for this publication at: https://www.researchgate.net/publication/272129062

Hydrogen bonding of water confined in zeolites and their zeolitic imidazolate framework counterparts

ARTICLE *in* RSC ADVANCES · JUNE 2014

Impact Factor: 3.84 · DOI: 10.1039/C4RA01508H

CITATIONS
2

READS
35

2 AUTHORS:

Sofia Calero
Universidad Pablo de Olavide
164 PUBLICATIONS **3,113** CITATIONS
SEE PROFILE

Paula Gómez-Álvarez
Universidad Pablo de Olavide
26 PUBLICATIONS **41** CITATIONS
SEE PROFILE

Available from: Paula Gómez-Álvarez
Retrieved on: 26 January 2016

RSC Advances

RSCPublishing

ARTICLE

Hydrogen bonding of water confined in zeolites and their Zeolitic Imidazolate Framework counterparts

S. Calero and P. Gómez-Álvarez*

Hydrogen bonds play a crucial role in the macroscopic behaviour of associated liquids. In particular, the singular properties of water are generally ascribed to the association at molecular level, and a significant number of works have been focused on gaining understanding of this subject. However, a consistent description of this phenomenon when confining water in nanoporous materials is still lacking. This work is aimed at elucidating the effect of confinement in various structures on the hydrogen bonding of water using molecular simulation techniques. In particular, we considered pure silica hydrophobic zeolites and in their respective Zeolitic Imidazolate Framework counterparts, which have larger pores and stronger affinity to water due to their chemical composition. Adsorption of water in these structures was computed via Monte Carlo simulations in the Grand-Canonical ensemble using previously validated force fields. A geometric criterion of hydrogen bonding formation was applied over generated configurations and allowed the computation of the structure of confined water. Our results at high hydration indicate considerable changes in relation to bulk water, which were found quite sensitive to the confining structure.

1 Introduction

Hydrogen bonding[1,2] in associated liquids has been systematically studied for many years. Although several techniques such as neutron and X-ray diffraction have considerably increased our knowledge of their structural properties, no accurate and unambiguous information can be extracted from experimental data. On the other hand, Molecular Simulation (MS) represents a powerful tool to complement experimental approaches and overcome their deficiencies since it allows a more detailed exploration of the molecular arrangements inside the fluid. The increasing computation power available to scientists has made MS a very useful alternative to gain further insight into the details of the hydrogen-bonding structure of associated substances. This interest is due to the fact that hydrogen-bonded (HB) interactions play a crucial role in many chemical and biological processes, and are responsible of a number of peculiar properties observed in these systems. In this respect, water[3,4] has been studied more extensively than any other liquid, both experimentally[5-12] and computationally.[13-29] It is well-known that bulk liquid water shows a complicated tetrahedral HB network, the variation of which as a function of temperature and pressure provokes the singular macroscopic behaviour. However, a significant number of its properties remain partially unknown. Among them, there are the properties related to water in confinement. The molecular-level characterization of the structure of water within the nanopore is key to understanding many processes of relevance in a variety of fields, from a scientific point of view to industrial applications such as catalysis, biological membrane transport, removal of pollutants from water or oil recovery. In the last decade, several studies[30-58] of the structural and dynamical properties of water in different spatially restricted environments have been reported, showing that confined water exhibits different properties than bulk water. Most of these works deal with water adsorbed on simple cylindrical[32-42] or slit-shaped[43-51] geometries, both carbons and silicas, for various pore diameters, hydration levels and thermodynamic conditions. However, little is known about the microscopic behaviour of water during adsorption in porous materials.[52-59]

In recent years, the number of available nanoporous materials has increased substantially, with new material classes such as Metal-Organic Frameworks (MOFs) joining the traditional adsorbents, which include activated carbons, porous silicas, and zeolites. Zeolites are nanoporous crystalline

structures formed by covalently bonded TO_4 tetrahedra, where the T central atoms are usually silicon or aluminum atoms. These primary units join to form groups of simple polyhedra which merge in turn to form a three-dimensional system of cavities of molecular dimensions (3 to 12 Å). While the introduction of AlO_4 units induces a negative net charge in the structure that has to be balanced by non-framework cations, pure silica zeolites are charge neutral. On the other hand, MOFs are nanoporous materials consisting of metal centers coordinated to organic molecules that act as linkers to form extended three-dimensional networks. Due to the large choice of both the metal complex and the organic linker, a number of potential structures with a large variety in chemical compositions and pore sizes and shapes can be synthesized. However, these structures are quite unstable and they easily decompose upon heating or upon template removal; likewise, water can attack the metal centers and destroy the crystalline framework structure. Zeolitic Imidazolate Frameworks (ZIFs) are a class of MOFs having zeolite topologies in which tetrahedral atoms are replaced by transition metals (usually Zn or Co) and oxygen atoms by imidazolate units. Unlike most common MOFs, they have been found exceptionally chemical and thermal stable.[60]

This work is aimed at evaluating the hydrogen bond properties of water adsorbed in crystalline porous materials as well as elucidating the effect of the host topology and geometry. In this sense, we selected a series of all-silica zeolites and their ZIF counterparts. The pore sizes of the latter are approximately twice as large as those of their zeolite counterparts by virtue of the longer organic linkers. In particular, we considered the five industrially important FAU, FER, MFI, MOR, and RHO zeolites. The FAU-type pore structure consists of sodalite cages arranged in 12 Å wide supercages accesible through 7.2 Å windows. FER zeolite consists of straight 10-ring channels (5.4 × 4.2 Å) parallel to the z-axis which are interconnected by cages with 8-ring windows (4.8 × 3.5 Å) in the y-direction. The MFI-type zeolite is characterized by a three-dimensional pore system of longitudinal channels interconnected by zigzag channels of about 5.5 Å in diameter. Mordenite MOR has a 1-dimensional porous structure whose parallel channels have little cavities (side-pockets) all along them. Finally, RHO zeolite has two types of cavities, α and D8R, and a body centered cubic symmetry; the smallest effective canal diameter defined as the diameter of an eight-member ring is 3.6 Å.

Monte Carlo simulations in the Grand Canonical ensemble were carried out to compute the adsorption of water in all the structures at room temperature. The structure of confined water has been described in terms of the Radial Distribution Functions (RDFs) and the HB statistics. In particular, the following properties were determined on the basis of a specific criterion of hydrogen bonding formation applied along the simulation: The fraction of monomers and associated molecules, the fraction of the latter involved in 1-5 hydrogen bonds (f_1, f_2, f_3, f_4, f_5), and the resulting average number of bonds per molecule n_{HB}. An analysis of the water clustering was likewise addressed.

The paper is organized as follows. The methods are described in section 2. In section 3, the results on thermodynamics and structural properties of confined water are collected and comprehensively discussed. Finally, the main results are contained in the concluding section 4.

2 Methods

2.1 Structures

The zeolite topologies were extracted from the International Zeolite Association (IZA) database[61] and optimized by lattice energy minimization using GULP[62] with Sanders *et al.*[63] potentials to model the Si-O interactions. In a second stage, these minimized zeolite structures were converted to Zn and imidazole based ZIFs by applying TOBUNPOROUS,[64,65] a code written to: (i) replace each Si centre with a metal unit, here Zn; (ii) replace the bridging oxygen of the Si-O-Si bridge by a linking ligand, here bare imidazole; and finally (iii) scale the unit-cell dimensions appropriately. The resulting structures were relaxed using DL POLY[66] through the Conjugate Gradient (CG) minimization algorithm. Figure 1 illustrates the atomic structure of both the zeolite and ZIF forms for the specific case of MOR; these for the remaining topologies are included in Figures S1-S4 of the Electronic Supporting Information (ESI).

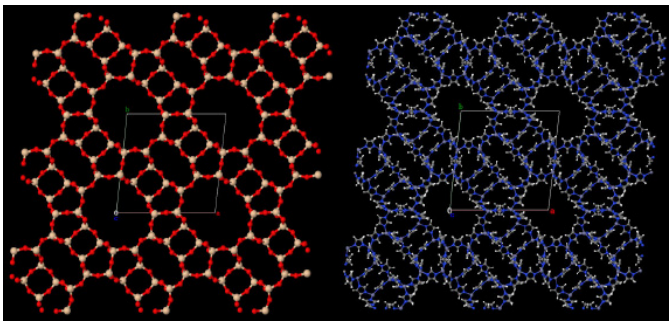

Fig. 1 Zeolite and ZIF forms of MOR topology.

2.2 Models and force fields

The host structures were treated as rigid frameworks. Guest water molecules were described by the TIP5P/Ew model,[67] a TIP5P model parameterized for Ewald sums. It is a rigid five-site potential: The oxygen (O), the two hydrogen atoms (H) and two extra dummy atoms (M) with tetrahedral site distribution with the O at the centre. There is only a single dispersive center at the O atom, and point charges are located at the H and M sites, the latter accounting for the negative partial charge of the oxygen atom. The geometry and model parameters are summarized in Figure S5 of the ESI. We selected this particular model since it has been proved suitable for studying adsorption of water in zeolites.[68] For bulk liquid water, several other models[69-71] have also been considered in order to compare results from the hydrogen bonding calculations.

The interactions between framework atoms and water are defined through both Lennard-Jones and Coulombic potentials. In the case of zeolites, every silicon atom is surrounded by four oxygen atoms, and so the latter dominate the dispersive forces between the water molecules and the structure. For this reason, only effective dispersive interactions with framework oxygen atoms are taken into account. The considered L-J cross-potential parameters were ε/k_B [K] = 13.71 K and σ [Å] = 3.3765 Å.[72] The lattices were assumed with static atomic charges with q_{Si} = 0.78598 e^-.[73] Each oxygen atom is assigned to half the charge of the silica atoms with opposite sign to preserve the electrostatic neutrality of the structure: q_O = -0.39299 e^-. As for ZIFs, the Lennard-Jones parameters for the framework atoms were taken from the DREIDING[74] generic force field except those of Zn, which corresponds to the UFF.[75] These values were implemented together with Lorentz-Berthelot mixing rules[76] to compute the interactions with water molecules. The partial charges were taken from the work of Gutiérrez-Sevillano *et al*.[77]

2.3 Simulation details

Using the above-described models and force fields, Monte Carlo simulations of water at room temperature were performed using the RASPA code developed by D. Dubbeldam, S. Calero, D. E. Ellis, and R. Q. Snur.[78,79] The adsorption of water in the structures was computed using the Grand-Canonical ensemble (μVT), in which temperature, volume and chemical potential are kept fixed. The chemical potential μ is related to the imposed fugacities, from which pressures can be determined using the Peng-Robison equation of state.[80] The number of unit cells for each structure was chosen in order to get a simulation box larger than twice the Lennard-Jones cut-off radius, which was set to 12 Å. Periodic boundary conditions[76] were employed. The long-range electrostatic interactions were evaluated using Ewald summation technique.[76] Simulations were arranged in cycles of trial moves including molecular translation, rotation, and insertion or deletion of a molecule. Each point of the isotherms was obtained after equilibration runs of 50 000 cycles followed by production runs of 500 000 cycles. Finally, it is worth noting that all the pores of the zeolite lattices under study are accessible for water molecules (kinetic diameter 2.68 Å), and so no artificial blocks were needed in our simulations. Simulations in the isothermal–isobaric ensemble (NpT) were also carried out for calculating the properties of bulk liquid water. In these simulations, a fixed number of 500 particles are placed in a cubic box with an initial length of 30 Å. In this case, moves in each cycle include translation, rotation, and volume changes. Usual long-range corrections[76] were used for Lennard-Jones interactions and the Ewald summations for the electrostatic ones.

For an accurate estimation of the number of hydrogen bonds between water molecules, one needs to apply a rigorous criterion. Following the literature, various criteria have been developed for exploring hydrogen bonds on the basis of energetic[13] and geometric[14,17] conditions. Hybrid criteria by both energy and geometry are also utilized.[25] In this work, the HB network of water in each state (bulk and confined in the different pore systems) has been studied in terms of the relative configuration of two water molecules. According to the geometric criterion, a hydrogen bond between two water molecules exists when their interatomic separations r_{OO} and r_{OH} are lower than certain cut-off values, which are given by the respective average distances of the first minimum location in the g_{OO} and g_{OH} functions, and limitation[17] to the angle α between intermolecular O-O vector and covalent O-H vector is fulfilled.

3 Results

To establish a relation with the results of this study, a number of properties characterizing the targeted structures were computed using Zeo++,[81] a software package for analysis of crystalline porous materials. Table 1 collects the values of framework density, Pore Limiting Diameter (PLD), Largest Cavity Diameter (LCD), and accessible volumes (AV) and surface areas (ASA). Note that the last two magnitudes are a function of the size of the guest molecules. The reported values correspond to water adsorption. We likewise computed Pore Size Distributions (PSDs), which are displayed in Figure S6 of the ESI.

Table 1 Properties of the frameworks under study.

	Density / kg·m^{-3}	PLD / Å	LCD / Å	AV / cm^3·g^{-1}	ASA / m^2·g^{-1}
Zeolites					
FAU	1347	6.76	10.59	0.17	1108
FER	1842	4.23	5.65	0.03	633
MFI	1816	4.69	6.47	0.04	694
MOR	1772	5.82	6.26	0.05	704
RHO	1486	3.49	9.84	0.11	1145
ZIFs					
FAU	556	13.62	20.86	0.87	3282
FER	816	7.93	10.02	0.30	3059
MFI	795	9.00	11.88	0.34	3165
MOR	780	10.82	11.52	0.35	3169
RHO	601	8.13	20.08	0.70	3514

Figure 2 shows the adsorption isotherms of water in the structures at 298.15 K. Regarding zeolites, it must be noted that the experimental lattices[82-86] have been also considered, but negligible variations in the results with respect to those obtained using the optimized IZA structures were found. Therefore, only results for the latter were included.

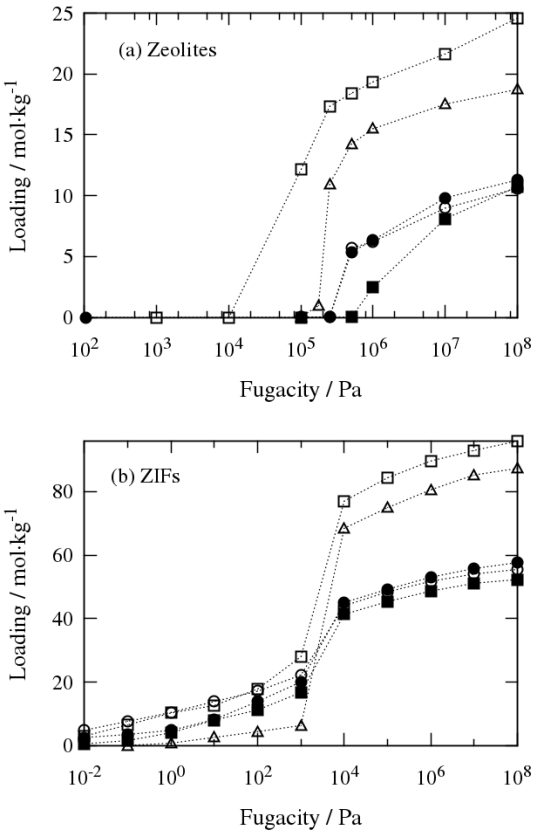

Fig. 2 Simulated adsorption isotherms of water in (a) zeolites and (b) their ZIF counterparts at 298.15 K on logarithmic scale. FAU (empty square), FER (full square), MFI (empty circle), MOR (full circle), and RHO (triangle). Lines are guides to the eye.

On the one hand, molecular simulations predict that essentially no water molecules adsorb in the pure silica zeolites up to a threshold pressure. Water intrusion is a first order vapour–liquid transition that takes place above bulk saturation pressure (p_0=3.2 kPa at 298 K). This behaviour is typical of hydrophobic solids and agrees with previously reported works.[87,88] Both the onset pressure of water intrusion and the saturation capacity are clearly dependent on the pore arrangement. In particular, the earliest adsorption and highest loadings occur in FAU and RHO, which are cage-like structures with the highest pore volumes. The similarity among the isotherm curves of the remaining zeolites is consistent with their pore geometry and accessible space. On the other hand, the adsorption of water in ZIFs differs considerably from that in their respective zeolite counterparts. Their higher affinity to water allows adsorption in the gas phase. A steep condensation transition at values of fugacity in the order of p_0 is observed for all ZIFs. This behaviour is in agreement with previous computational studies.[89] Large water uptakes with respect to the zeolites are determined from their more and larger pores. Indeed, the variation in the adsorption capacity from zeolite to ZIF for a fixed topology is in close relation to that in the pore volume.

To give an idea of the molecular packing at each state, the density of water in the structures is plotted as a function of the fugacity in Figure 3. It is defined as the relation between the adsorbed molecules and the effective volume of the framework determined by taking its porosity into account. The higher the fugacity, the larger the water coverage and so the density. Results at high hydration are consistent. Adsorption from the gas phase strongly depends on pore-water interactions, and for attractive forces (although weaker than those between water molecules), the density of the confined water is larger than that of the bulk water. Figure 4 shows the average occupation profile of water for MOR zeolite and selected values of fugacity as illustrative example of the molecular packing.

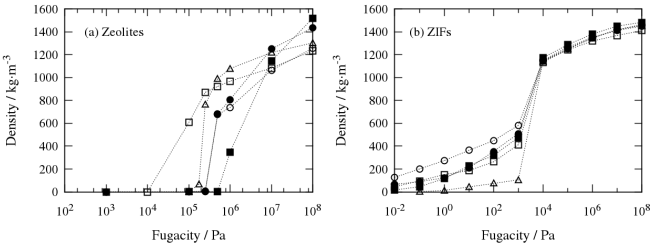

Fig. 3 Density of water in (a) zeolites and (b) their ZIF counterparts as a function of the fugacity at 298.15 K on logarithmic scale. FAU (empty square), FER (full square), MFI (empty circle), MOR (full circle), and RHO (triangle). Lines are guides to the eye.

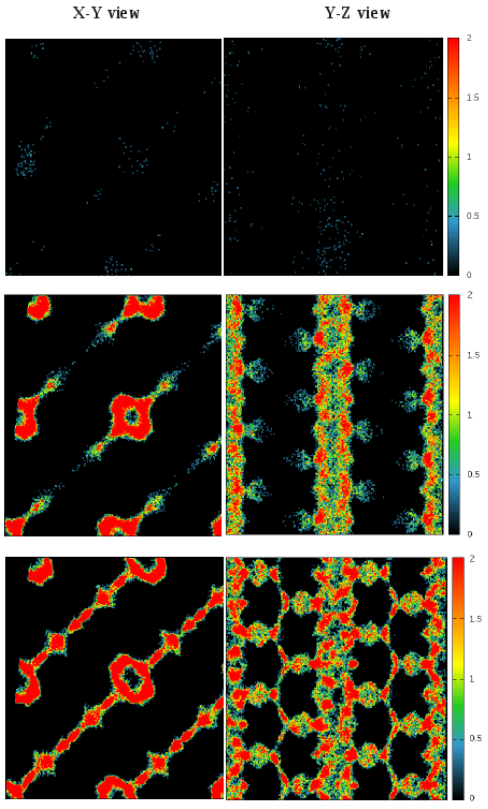

Fig. 4 Average occupancy profiles of water in MOR zeolite over X-Y and Y-Z planes at 0.25 MPa (top), 1 MPa (middle) and 100 MPa (bottom). The relation between colour and probability density occupation (from blue to red) is shown in the bar colour ramp situated on the right side of the figure.

The study of the structure of the confined water states follows. In section 3.1, we report the simulated radial distribution functions and section 3.2 is devoted to the HB statistics and cluster analysis.

3.1 Radial Distribution Functions

The analysis of the Radial Distribution Functions (RDFs) helps to understand the microscopic behaviour of the water molecules inside the porous materials by providing information on the average intermolecular distance and the presence of hydrogen bonding. The O-O and O-H RDFs of water in the zeolites and ZIFs, as well as the results corresponding to the bulk, are given in Figures S7-S9 of the ESI. The behaviour of $g_{OO}(r)$ and $g_{HO}(r)$ reveals the existence of water association regardless of the host structure. The positions of the first peaks and minima remain unchanged in relation to bulk liquid water. This is a clear indication of stable hydrogen bonding. However, a redistribution of the nearest neighbours of confined water is deduced from a number of aspects such as the absence of the second maximum of goo(r) characterizing the tetrahedral ordering of water molecules due to hydrogen bonding in the bulk. Conversely, the second peak of $g_{OH}(r)$ is kept. Concerning the intensity of the peaks, notably high maxima are observed for water in zeolites at the lowest values of fugacity due to the low uptake.

3.2 HB statistics and cluster analysis

According to the widely used "distance-angle" definition[17-19] for hydrogen bonding in bulk liquid water, a bond is taken to exist between a pair of molecules if 1) the respective oxygen atoms are separated by less than 3.6 Å, 2) the oxygen of the acceptor molecule and the hydrogen of the donor are separated by less than 2.4 Å, and 3) the α angle is less than a threshold value, usually 30º, to account for linear hydrogen bonds. These cut-off values for distances correspond to the positions of the first minima in the respective radial distribution functions. As these positions were found invariant for water confined in all the structures, we conclude that this criterion is also applicable for the study in this work. The number of monomers and associated molecules in the simulation cell (s. c.) computed for each state on the basis of this geometric criterion is shown in Figure 5. As can be observed, most guest water molecules are hydrogen-bonded; the presence of monomers is negligible, especially for FAU topology. However, despite most molecules appear associated, our findings on the average number of bonds per molecule n_{HB} and HB populations reveal a significantly different structure from the bulk. The estimated error in these magnitudes is always lower than 5 percent.

Results concerning n_{HB} for water in the bulk and in confinement are presented in Table 2 and Figure 6, respectively. The n_{HB} value for bulk water using TIP5P/Ew[67] was found about 3.2. Note that this value is slightly lower than those obtained by models with four interacting sites.[69-71] This is likely the key of that difference and suggests limitations of developing H-bond interactions as a consequence of the 5 site-based tetrahedral geometry of the molecule. The results reflect the typical tetrahedral HB network of bulk liquid water and are in consistency with those of previous works based on molecular simulation.[18-21]

Fig. 5 Number of total (red), associated (blue), and monomer (green) water molecules in (a) zeolites and (b) their ZIF counterparts as a function of the fugacity at 298.15 K. Lines are guides to the eye.

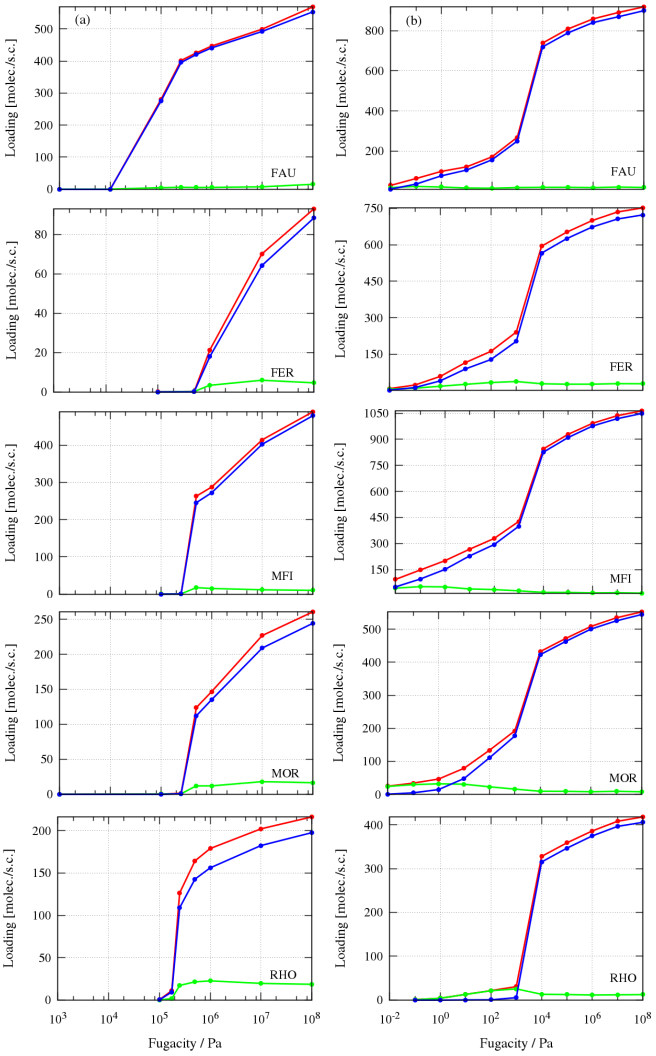

Table 2 HB statistics of bulk liquid water defined by various models.

	f_1	f_2	f_3	f_4	f_5	n_{HB}
TIP5P/Ew[67]	3.9	17.4	38.3	38.0	2.4	3.18
TIP4P[69]	1.9	12.1	36.0	45.4	4.6	3.39
TIP4P/Ew[70]	1.2	9.3	33.2	51.6	4.7	3.49
TIP4P/2005[71]	1.0	8.6	32.2	53.3	4.9	3.52

As shown in Figure 6, an increase with fugacity of n_{HB} from about 1, which indicates the mostly presence of dimers, to values between 2 and 3 depending on the structure is found. This denotes an enhancement of the hydrogen bonding with increasing water uptake. For similar loadings, the degree of association is larger in zeolites than in their ZIF counterparts. This is likely due to their smaller pore volumes and to the weak interactions with their hydrophobic surface. For similar water densities, the average number of bonds per molecule is, however, higher in ZIFs since the effect of the framework volume is taken into account. The results are also strongly dependent on the pore arrangement. In particular, water is the highest associated in FAU, followed by MFI. Likewise, the variation of n_{HB} with fugacity for water in both types of crystalline porous materials is closely related with the previously commented adsorption behaviour. In particular, the abrupt condensation transition in ZIFs at about 10^4 Pa is clearly reflected in the molecular association by increasing n_{HB} in a considerable extent. However, a clear weakening of the hydrogen-bonded network of confined water when structures are highly hydrated in relation to bulk liquid (n_{HB} = 3.18) is observed.

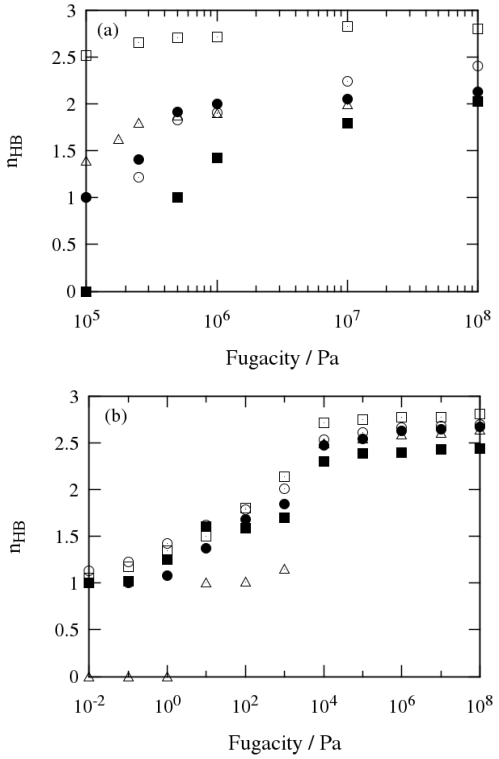

Fig. 6 Average number of hydrogen bonds n_{HB} as a function of the fugacity for water confined in (a) zeolites and (b) their ZIF counterparts at 298.15 K. FAU (empty square), FER (full square), MFI (empty circle), MOR (full circle), and RHO (triangle). The error in the reported values is smaller than the symbol size.

The distribution f_i of water molecules with *i* hydrogen bonds is given in Table 3. The values corresponding to zeolites were found to be very stable from the lowest adsorption pressures due to the rapid pore filling. Regarding ZIFs, a clear modification of these data is observed from the vapour-liquid transition. At the lowest values of fugacity, the highest percentages correspond to molecules engaged in 1 hydrogen bond for either zeolites or ZIFs. At high values of fugacity, our calculations reveal a considerably lower fraction of molecules involved in 4 hydrogen bonds with respect to the bulk (Table 2) in favour to molecules with 1 and 2 HBs. Thus, the confinement prevents the tetrahedral H-bonding network regardless of the host structure in agreement with literature on simple confining geometries. Instead, molecules tend to form chain-like clusters. This is due to the important amount of molecules in contact with the extended surface. To gain insights into this issue, we computed the number of water molecules near the surface of the pores and of bulky molecules for the highest value of fugacity. To this end, we considered a bound state when the distance of the oxygen of water molecule from the framework atom is lower than the corresponding value of σ parameter; otherwise, it is a free water molecule. The percentage of the latter is given in Table 4. As it is apparent from the values, the large pores of ZIFs lead to a considerable proportion of bulky molecules. Among the studied zeolites, FAU and RHO also show a non-negligible relative uptake of bulky molecules. This can be explained in terms of their cage-like structures with large adsorption capacities.

For a fixed topology, the degree of association increases with the available space within the nanopore since the tendency to form hydrogen bonds increases with increasing the number of neighbouring molecules. This fact is apparent from the HB results of water in zeolites and their respective ZIFs at complete filling. The approximately twice larger pores of the latter lead to highly structured water, except for FAU. This point leads to conclude that, when the confining nanopores are large enough, (1) an increase of the pore sizes hardly affects the structure of confined water; and (2) the nature of the surface interaction forces induced by the framework composition is not an influencing factor on the weakening of hydrogen bonding with respect to the bulk state. It is primarily a purely geometrical effect. As can be deduced from data in Table 3 and Table 1, the HB structure of confined water is, however, not unambiguously associated with the accessible space of the host structures. The HB distribution of water in RHO zeolite denotes a surprisingly weaker structure than that in FAU despite their similar characteristics. Indeed, the results are virtually coincident with these for FER and MOR although RHO has approximately twice larger values of accessible surface and volume. This can be due to a breaking of hydrogen bonds promoted by its small windows connecting the cavities, with the lowest limiting diameter of the considered zeolites. The opposite holding occurs for MFI zeolite. While it has similar pore properties to FER and MOR, we found higher values of f_3 in detriment to f_1, and so a more complex molecular network. This is likely due to the cages formed by the intersections between longitudinal and zigzag channels, which could act as sites of strengthening of molecular cohesion of water. These findings denote a great influence of the pore geometry and framework topology on the HB formation between adsorbed water molecules.

Table 3 Percentages f_i of confined water molecules involved in i hydrogen bonds as a function of fugacity for each structure.

FAU

Zeolite						ZIF					
Fugacity / MPa	f_1	f_2	f_3	f_4	f_5	**Fugacity / Pa**	f_1	f_2	f_3	f_4	f_5
0.1	14.1	34.5	37.6	13.1	0.6	10^{-2}	94.5	5.4	0.1	0.0	0.0
0.25	10.5	31.9	39.9	16.7	1.0	10^{-1}	84.3	14.1	1.5	0.1	0.0
0.5	9.6	30.1	40.9	18.2	1.1	1	69.0	27.4	3.2	0.4	0.0
1	9.5	30.4	40.4	18.4	1.3	10	59.2	32.9	6.7	1.3	0.0
10	8.2	26.8	41.3	21.8	1.9	10^{2}	44.4	36.6	14.1	4.2	0.7
100	10.6	25.1	39.9	22.1	2.2	10^{3}	32.5	32.8	24.6	8.8	1.3
						10^{4}	11.7	29.9	35.0	21.9	1.4
						10^{5}	11.9	27.9	35.5	22.6	2.2
						10^{6}	11.2	27.9	35.9	22.4	2.6

FER

Zeolite						ZIF					
Fugacity / MPa	f_1	f_2	f_3	f_4	f_5	**Fugacity / Pa**	f_1	f_2	f_3	f_4	f_5
0.5	100.0	0.0	0.0	0.0	0.0	10^{-2}	100.0	0.0	0.0	0.0	0.0
1	58.4	40.6	1.0	0.0	0.0	10^{-1}	98.0	2.0	0.0	0.0	0.0
10	39.6	42.2	17.1	1.1	0.0	1	78.9	17.3	3.0	0.8	0.0
100	29.5	42.3	24.4	3.7	0.1	10	55.4	33.0	8.2	2.6	0.8
						10^{2}	56.5	30.5	10.4	2.3	0.3
						10^{3}	48.3	36.3	12.9	2.5	0.1
						10^{4}	22.4	37.1	28.4	11.8	0.4
						10^{5}	19.9	35.7	30.9	12.8	0.7
						10^{6}	20.3	34.9	30.7	13.1	1.0

MFI

Zeolite						ZIF					
Fugacity / MPa	f_1	f_2	f_3	f_4	f_5	**Fugacity / Pa**	f_1	f_2	f_3	f_4	f_5
0.01	100.0	0.0	0.0	0.0	0.0	10^{-2}	86.9	12.9	0.2	0.0	0.0
0.25	77.7	22.3	0.0	0.0	0.0	10^{-1}	79.6	18.5	1.9	0.0	0.0
0.5	35.0	48.3	14.8	1.8	0.0	1	64.8	28.9	5.6	0.7	0.0
1	31.0	49.2	17.5	2.2	0.0	10	51.7	35.9	10.3	1.9	0.1
10	20.1	42.7	30.4	6.5	0.2	10^{2}	42.4	39.4	15.5	2.4	0.2
100	15.6	38.3	36.1	9.5	0.5	10^{3}	31.2	40.9	23.5	4.3	0.1
						10^{4}	14.5	34.7	34.0	16.1	0.7
						10^{5}	12.8	32.8	35.8	17.5	1.1
						10^{6}	11.5	32.6	35.8	18.5	1.6

MOR

Zeolite						ZIF					
Fugacity / MPa	f_1	f_2	f_3	f_4	f_5	**Fugacity / Pa**	f_1	f_2	f_3	f_4	f_5
0.1	100.0	0.0	0.0	0.0	0.0	10^{-2}	100.0	0.0	0.0	0.0	0.0
0.25	63.0	33.1	3.6	0.3	0.0	10^{-1}	99.2	0.8	0.0	0.0	0.0
0.5	35.3	41.4	19.9	3.4	0.1	1	93.5	5.1	0.9	0.5	0.0
1	32.4	40.2	22.8	4.5	0.1	10	71.9	21.5	4.1	2.4	0.0
10	32.1	38.2	23.0	6.3	0.5	10^{2}	47.8	39.3	9.6	3.2	0.1
100	28.6	39.3	23.6	7.6	0.9	10^{3}	37.0	45.0	14.7	3.3	0.0
						10^{4}	14.6	38.0	33.2	13.7	0.5
						10^{5}	13.4	36.1	34.0	15.5	1.0
						10^{6}	11.8	33.6	36.1	17.1	1.3

RHO

Zeolite						ZIF					
Fugacity / MPa	f_1	f_2	f_3	f_4	f_5	**Fugacity / Pa**	f_1	f_2	f_3	f_4	f_5
0.1	62.0	37.2	0.8	0.0	0.0	1	0	0	0	0	0
0.175	49.0	40.5	9.7	0.8	0.0	10	100.0	0.0	0.0	0.0	0.0
0.25	41.5	39.3	17.1	2.1	0.0	10^{2}	98.9	1.1	0.0	0.0	0.0
0.5	38.6	39.1	18.9	3.2	0.2	10^{3}	87.1	11.2	1.7	0.1	0.0
1	38.0	38.0	20.1	3.7	0.2	10^{4}	17.4	33.3	32.9	15.6	0.8
10	33.3	39.0	22.7	4.7	0.3	10^{5}	16.0	32.7	33.7	16.4	1.2
100	32.0	39.4	22.9	5.3	0.3	10^{6}	15.0	32.2	34.1	16.7	2.0

Table 4 Percentage of bulky (free) water molecules in each structure at high hydration.

% free	FAU	FER	MFI	MOR	RHO
Zeolite	28.7	4.0	1.9	3.1	15.9
ZIF	54.3	21.6	24.1	23.4	42.2

Finally, the water aggregates formed in the highly hydrated structures were evaluated in terms of the cluster size distribution. Results are collected in Figure S10 of the ESI. Short aggregates are the most probable in FER, MOR, and RHO zeolites. Although this is also the case in the ZIFs and FAU and MFI zeolites, the formation of an extended H-bonded network composed by almost all adsorbed water molecules in these structures is clearly apparent from the inset figures. This clustering is in agreement with previous comments on HB statistics.

4 Conclusions

A detailed description of the H-bonded structure of water adsorbed in zeolites and ZIF porous materials has been reported using Monte Carlo simulations with validated atomistic descriptions and intermolecular interactions. The consistency of the obtained adsorption isotherms with literature points to the reliability of the thermodynamics. The calculated hydrogen bonding properties are in close relation to the adsorption behaviour. While the adsorption mechanism in all-silica zeolites proceeds through nucleation of water molecules, the degree of association gradually increases in ZIFs up to condensation, where a considerable enhancement of hydrogen bonding is observed. For saturated states, our simulations proved that water is significantly perturbed from its bulk behaviour. Although association is still very important, a loss of the tetrahedral ordering typical of bulk liquid water is observed. Instead, water molecules form aggregates whose nature was found notably sensitive to the type of confining structure. Overall, the molecular association is favoured by large pore sizes and volumes, but is not unambiguously associated with these features. In particular, the more extended and complex HB networks were found in ZIFs, and FAU and MFI zeolites. The large cavities and accessible space of ZIFs and FAU zeolite are unquestionably, but MFI has similar pore properties to FER and MOR. Its intersecting channel-like topology could be the key point on this finding. Likewise, despite its large cages, the connectivity by small windows in RHO zeolite prevents the formation of high order clusters.

This work represents a step forward on the association at molecular scale governing the behaviour of water in nanoporous materials. Although it has been focused on the influence of host geometric and topological characteristics on water-water hydrogen bonds, it would be worthwhile to further investigate interaction forces with the pore surface. Likewise, to extend this study at different temperatures would be interesting for a deeper understanding of the phenomena concerned with the modification of hydrogen bonding of confined water.

Acknowledgements

This work is supported by the European Research Council through an ERC Starting Grant (ERC2011-StG-279520-RASPA).

* E-mail: pgomalv1@upo.es

[a] Department of Physical, Chemical, and Natural Systems. University Pablo de Olavide. Ctra. Utrera km 1, 41013, Seville. Spain.

†Electronic Supplementary Information (ESI) available: [Figures of lattice topologies, water model, Pore Size Distributions of the structures, Radial Distribution Functions, and cluster size distributions]. See DOI: 10.1039/b000000x/

References

1 E. Arunan, G. R. Desiraju, R. A. Klein, J. Sadlej, S. Scheiner, I. Alkorta, D. C. Clary, R. H. Carbtree, J. J.Dannenberg, P. Hobza, H. G. Kjaergaard, A. C. Legon, B. Mennucci and D. J. Nesbitt. *Pure Appl. Chem.*, 2011, **83**, 1619.

2 L. Pauling, *The Nature of the Chemical Bond*, Cornell University Press, New York, 1948.

3 D. Eisenberg and W. Kauzmann, *The Structure and Properties of Water*, Oxford University Press, London, 1969.

4 F. Franks, *Water: A Comprehensive Treatise*, Plenum Press, New York, 1972.

5 A. H. Narten, W. E. Thiessen and L. Blum, *Science*, 1982, **217**, 1033-1034.

6 O. Conde and J. Teixeira, *Mol. Phys.*, 1984, **53**, 951-959.

7 J. L. Rousset, E. Duval and A. Boukenter, *J. Chem. Phys*., 1990, **92**, 2150-2154.

8 J. C. Dore, *J. Mol. Struct.*, 1991, **250**, 193-211.

9 K. Ichikawa, Y. Kameda, T. Yamaguchi, H. Wakita and M. Misawa, *Mol. Phys.*, 1991, **73**, 79-86.

10 E. W. Castner, Y. J. Chang, Y. C. Chu and G. E. Walrafen, *J. Chem. Phys.*, 1995, **102**, 653-659.

11 Y. E. Gorbaty, G. V. Bondarenko, A. G. Kalinichev and A. V. Okhulkov, *Mol. Phys*., 1999, **96**, 1659-1665.

12 J. Urquidi, S. Singh, C. H. Cho and G. W. Robinson, *Phys. Rev. Lett.*, 1999, **83**, 2348-2350; *J. Mol. Struct.*, 1999, **485-486**, 363-371.

13 A. Rahman, and F. H. Stillinger, *J. Chem. Phys*., 1971, **55**, 3336; A. Geiger, F. H. Stillinger and A. Rahman, *J. Chem. Phys.*, 1979, **70**, 4185-4193.

14 M. Mezei and D. L. Beveridge, *J. Chem. Phys.*, 1981, **74**, 622-632.

15 M. Ferrario, M. Haughney, I. R. McDonald and M. L. Klein, *J. Chem. Phys*., 1990, **93**, 5156-5166.

16 I. M. Svishchev and P. G. Kusalik, *J. Chem. Phys.*, 1993, **99**, 3049-3058.

17 A. Luzar and A. Chandler, *Phys. Rev. Lett.*, 1996, **76**, 928-931; *Nature* (London), 1996, **379**, 53-57; *J. Chem. Phys*., 1993, **98**, 8160-8173.

18 J. Martí, J. A. Padro and E. Guàrdia. *J. Chem. Phys*., 1996, **105**, 639-649.

19 J. Martí, *J. Chem. Phys*., 1999, **110**, 6876- 6886.
20 A. G. Kalinichev and J. D. Bass, *J. Phys. Chem. A*, 1997, **101**, 9720-9727.
21 A. G. Kalinichev and S. V. Churakov, *Fluid Phase Equilib.*, 2001, **183–184**, 271–278; *Chem. Phys. Lett.*, 1999, **302**, 411–417.
22 A. De Santis, A. Ercoli and D. Rocca, *J. Chem. Phys*., 1999, **111**, 4635-4639.
23 D. Marx, M. E. Tuckerman, J. Hutter and M. Parrinello, *Nature* (London), 1999, **397**, 601-604.
24 P. Jedlovszky, M. Mezei and R. Vallauri, *Chem. Phys. Lett.*, 2000, **318**, 155-160.
25 D. Swiatla-Wojcik, *J. Chem. Phys*., 2007, **342**, 260-266, and references therein.
26 D. Swiatla-Wojcik, A. Pabis and J. Szala, *Cent. Eur. J. Chem.*, 2008, **6**, 555–561.
27 R. Kumar, J. R. Schmidt and J. L. Skinner, *J. Chem. Phys*., 2007, **126** (204107), 1-12.
28 M. Matsumoto, *J. Chem. Phys.*, 2007, **126** (054503), 1-6.
29 H. Ma and J. Ma, *J. Chem. Phys.*, 2011, **135** (054504), 1-8.
30 J. Dore, *Chem. Phys*., 2000, **258**, 327-347.
31 N. E. Levinger, *Science*, 2002, **298**, 1722-1723.
32 I. Hanasaki, and A. Nakatani, *J. Chem. Phys*., 2006, **124**, 174714.
33 M. C. Gordillo, and J. Martí, *Chem. Phys. Lett*., 2000, **329**, 341-345; *Chem. Phys. Lett.,* 2001, **341**, 250-254.
34 C. Calero, M. C. Gordillo, and J. Martí, *J. Chem. Phys*., 2013, **138**, 214702.
35 O. Byl, J.-C. Liu, Y. Wang, W.-L.Yim, J. K. Johnson, and J. T. Yates, *J. Am. Chem. Soc.*, 2006, **128**, 12090-12097.
36 K. Shirono, and H. Daiguji, *J. Phys. Chem. C,* 2007, **111**, 7938-7946.
37 Q. Zhang, K.-Y. Chan, and N. Quirke, *Mol. Sim.*, 2009, **35**, 1215-1223.
38 A. Giaya, and R. W. Thompson, *J. Chem. Phys.,* 2002, **117**, 3464-3475.
39 M. Rovere, M. A. Ricci, D. Vellati, and F. A. Bruni, *J. Chem. Phys.,* 1998, **108**, 9859-9867.
40 C. Hartnig, W. Witschel, E. Spohr, P. Gallo, M. A. Ricci, and M. Rovere, *J. Mol. Liq.*, 2000, **85**, 127-137.
41 P. Gallo, M. A. Ricci, and M. Rovere, *J. Chem. Phys*., 2002, **116**, 342 -346.
42 A. A. Milischuk, and B. M. Ladanyi, *J. Chem. Phys*., 2011, **135**, 174709.
43 M. C. Gordillo, and J. Martí, *J. Chem. Phys*., 2002, **117**, 3425-3430.
44 J. Marti, J. Sala, E. Guardia, and M. C. Gordillo, *Phys. Rew. E*, 2009, **79**, 031606.
45 M. C. Gordillo, and J. Marti, *J. Phys.:Condens. Matter*, 2010, **22**, 284111.
46 J. Marti, J. Sala, and E. Guardia, *J. Mol. Liq.*, 2010, **153**, 72-78.
47 S. H. Lee, and P. J. Rossky, *J. Chem. Phys.,* 1994, **100**, 3334-3345.
48 E. Spohr, A. Trokhymchuk, and D. Henderson, *J. Electroanal. Chem*., 1998, **450**, 281-287.
49 P. A. Bonnaud, B. Coasne, and R. J. M. Pellenq, *J. Phys.: Condens. Matter,* 2010, **22**, 284110.
50 M. O. Jensen, O. G. Mouritsen, and G. H. Peters, *J. Chem. Phys.,* 2004, **120**, 9729-9744.
51 P. Hirunsit, and P. B. Balbuena, *J. Phys. Chem. C,* 2007, **111**, 1709-1715.
52 S. Calero and P. Gómez-Álvarez, *J. Phys. Chem. C,* 2014, **118**, 9056-9065.
53 J. Puibasset, and R. J. M. Pellenq, *Eur. Phys. J. E,* 2003, **12**, S67-S70.
54 J. Puibasset, and R. J. M. Pellenq, *J. Chem. Phys.,* 2003, **119**, 9226-9232.
55 J. Puibasset, and R. J. M. Pellenq, *J. Phys.: Condens. Matter,* 2004, **16**, S5329-S5343.
56 F. Bruni, M. A. Ricci, and A. K. Soper, *J. Chem. Phys.,* 1998, **109**, 1478-1485; A. K. Soper, F. Bruni, and M. A. Ricci, *J. Chem. Phys*., 1998, **109**, 1486-1494.
57 N. Desbiens, A. Boutin, and I. Demachy, *Phys. Chem. B,* 2005, **109**, 24071-24076.
58 F.-X. Coudert, R. Vuilleumier, and A. Boutin, *ChemPhysChem.,* 2006, **7**, 2464-2467.
59 F.-X. Coudert, F. Cailliez, R. Vuilleumier, A. H. Fuchs, and A. Boutin, *Faraday Discussions,* 2009, **141**, 377-398.
60 K. S. Park, Z. Ni, A. P. Côté, J. Y. Choi, R. Huang, F. J. Uribe-Romo, H. K. Chae, M. O'Keeffe and O. M. Yaghi, *Proceedings of the National Academy of Sciences of the United States of America*, 2006, **103**, 10186-10191.
61 C. Baerlocher and L. B. McCusker, *Database of Zeolite Structures*, http://www.iza-structure.org/databases/.
62 J. D. Gale, *J. Chem. Soc. - Faraday Transac.*, 1997, **93**, 629-637; J. D. Gale and L. R. Andrew, *Mol. Sim.*, 2003, **29**, 291-341.
63 M. J. Sanders, M. Leslie and C. R. Catlow, *J. Chem. Soc., Chem. Commun*., 1984, 1271-1273.
64 A. R. Ruiz-Salvador and A. Gomez, *TOBUNPOROUS: Topological Building of Nanoporous Solids*, code available on request from the authors.
65 D. W. Lewis, A. R. Ruiz-Salvador, A. Gómez, L. M. Rodriguez-Albelo, F.-X. Coudert, B. Slater, A. K. Cheetham and C. Mellot-Draznieks, *CrystEngComm*, 2009, **11**, 2272-2276.
66 W. Smith and T. Forester, *J. Molec. Graphics*, 1996, **14**, 136-141.
67 S. Rick, *J. Chem. Phys.*, 2004, **120**, 6085-6093.
68 J. M. Castillo, D. Dubbeldam, T. J. H. Vlugt, B. Smit and S. Calero, *Mol. Sim.*, 2009, **35**, 1067-1076.
69 W. L. Jorgensen, J. Chandrasekhar, J. D. Madura, R. W. Impey and M. L. Klein, *J. Chem. Phys*., 1983, **79**, 926-935.
70 H. W. Horn, W. C. Swope, J. W. Pitera, J. D. Madura, T. J. Dick, G. L. Hura, and T. Head-Gordon, *J. Chem. Phys.*, 2004, **120**, 9665-9678.
71 L. F. Abascal and C. Vega, *J. Chem. Phys.*, 2005, **123,** 234505.
72 J. M. Castillo, J. Silvestre-Albero, F. Rodriguez-Reinoso, T. J. H. Vlugt and S. Calero, *Phys. Chem. Chem. Phys.*, 2013, **15**, 17374-17382.
73 A. García-Sánchez, C. O. Ania, J. B. Parra, D. Dubbeldam, T. J. H. Vlugt, R. Krishna and S. Calero, *J. Phys. Chem. C*, 2009, **113**, 8814-8820.
74 S. L. Mayo, B. D. Olafson and W. A. Goddard, *J. Phys. Chem*., 1990, **94**, 8897-8909.
75 A. K. Rappe, C. J. Casewit, K. S. Colwell, W. A. Goddard and W. M. Skiff, *J. Am. Chem. Soc.*, 1992, **114**, 10024-10035.
76 D. Frenkel and B. Smit, *Understanding Molecular Simulation*, Academic Press, San Diego, 1996.
77 J. J. Gutiérrez Sevillano, S. Calero, C. O. Ania, J. B. Parra, F. Kaptijn, J. Gascon and S. Hamad, *J. Phys. Chem. C*, 2013, **117**, 466-471.
78 D. Dubbeldam, A. Torres-Knoop and K. S. Walton, *Mol. Sim.*, 2013, **39**, 1253-1292.
79 D. Dubbeldam, S. Calero, D. E. Ellis and R. Q. Snurr, *RASPA 1.0: Molecular Software Package for Adsorption and Diffusion in Flexible Nanoporous Materials*, 2013.
80 D. B. Robinson, D. Y. Peng and S. Y. K. Chung, *Fluid Phase Equilib.*, 1985, **24**, 25-41.

81 T. F. Willems, C. H. Rycroft, M. Kazi, J. C. Meza and M. Haranczyk, *Microporous Mesoporous Mater.*, 2012, **149**, 134-141.

82 J. J. Hriljac, M. M. Eddy, A. K. Cheetham, J. A. Donohue and G. J. Ray, *J. Solid State Chem*., 1993, **106**, 66- 72.

83 R. E. Morris, S. J. Weigel, N. J. Henson, L. M. Bull, M. T. Janicke, B. F. Chmelka and A. K. Cheetham, *J. Am. Chem. Soc*., 1994, **116**, 11849-11855.

84 D. H. Olson, G. T. Kokotailo, S. L. Lawton and W. M. Meier, *J. Phys. Chem.*, 1981, **85**, 2238-2243.

85 V. Gramlich, Ph.D. Thesis, ETH, Zürich, Switzerland, 1971.

86 L. B. McCusker and Ch. Baerlocher, *Proc. 6th Int. Zeolite Conf*., 1984, 812-822.

87 F. Cailliez, M. Trzpit, M. Soulard, I. Demachy, A. Boutin, J. Patarin, and A. Fuchs, *Phys. Chem. Chem. Phys*., 2008, **10**, 4817-4826.

88 N. Desbiens, I. Demachy, A. H. Fuchs, H. Kirsch-Rodeschini, M. Soulard and J. Patarin, *Angew. Chem. Int. Ed*., 2005, **44,** 5310-5313.

89 A. U. Ortiz, A. P. Freitas, A. Boutin, A. H. Fuchs and F.-X. Coudert, *Phys. Chem. Chem. Phys*., 2014, **16**, 9940-9949.